# Two protonation switches control rhodopsin activation in membranes

Mohana Mahalingam[a], Karina Martínez-Mayorga[b,c], Michael F. Brown[c,1], and Reiner Vogel[a,2]

[a]Biophysics Section, Institute of Molecular Medicine and Cell Research, Albert Ludwigs University, Hermann-Herder-Strasse 9, D-79104 Freiburg, Germany; [b]Torrey Pines Institute for Molecular Studies, Fort Pierce, FL 34946; and [c]Department of Chemistry, University of Arizona, Tucson, AZ 85721

Edited by Wayne L. Hubbell, University of California School of Medicine, Los Angeles, CA, and approved September 22, 2008 (received for review May 9, 2008)

**Activation of the G protein-coupled receptor (GPCR) rhodopsin is initiated by light-induced isomerization of the retinal ligand, which triggers 2 protonation switches in the conformational transition to the active receptor state Meta II. The first switch involves disruption of an interhelical salt bridge by internal proton transfer from the retinal protonated Schiff base (PSB) to its counterion, Glu-113, in the transmembrane domain. The second switch consists of uptake of a proton from the solvent by Glu-134 of the conserved E(D)RY motif at the cytoplasmic terminus of helix 3, leading to pH-dependent receptor activation. By using a combination of UV–visible and FTIR spectroscopy, we study the activation mechanism of rhodopsin in different membrane environments and show that these 2 protonation switches become partially uncoupled at physiological temperature. This partial uncoupling leads to ≈50% population of an entropy-stabilized Meta II state in which the interhelical PSB salt bridge is broken and activating helix movements have taken place but in which Glu-134 remains unprotonated. This partial activation is converted to full activation only by coupling to the pH-dependent protonation of Glu-134 from the solvent, which stabilizes the active receptor conformation by lowering its enthalpy. In a membrane environment, protonation of Glu-134 is therefore a thermodynamic rather than a structural prerequisite for activating helix movements. In light of the conservation of the E(D)RY motif in rhodopsin-like GPCRs, protonation of this carboxylate also may serve a similar function in signal transduction of other members of this receptor family.**

FTIR spectroscopy | G protein-coupled receptor | ionic lock | membrane protein | UV–visible spectroscopy

G protein-coupled receptors (GPCRs) are 7-helical transmembrane proteins that exist in conformational equilibria between inactive and active conformations modulated by the binding of ligands (1). In the case of rhodopsin as a visual pigment, the ligand is the retinal chromophore, which is covalently linked to a lysine on transmembrane helix H7 by a protonated Schiff base (PSB) (2). The 11-*cis* retinal chromophore of the dark state is an inactivating inverse agonist that is converted by photoisomerization to the all-*trans* agonist, driving the conformational transitions leading to receptor activation. Within milliseconds several inactive intermediates are formed, such as Batho, BSI, Lumi, and Meta I, that can be examined by using time-resolved (3) or cryotrapping techniques (4). The early transitions involve mainly a relaxation of the isomerized retinal chromophore (5, 6), with only minor changes to the $\alpha$-helix bundle of the receptor protein as revealed by electron crystallography of the Meta I state (7). Only in the transition from Meta I to the active receptor conformation Meta II is a rearrangement of the helix bundle observed, involving tilt movements of H6 (8–10) and presumably also of H5 (11).

Activation of the receptor is proposed to involve 2 distinct protonation switches (Fig. 1*A*). The first switch entails disruption of a salt bridge between the retinal PSB on H7 and its complex counterion, consisting of Glu-113 on H3 and Glu-181 on extracellular loop 2 in the transmembrane part of the receptor (12), by deprotonation of the PSB and internal proton transfer to Glu-113 (13). The second switch is proton uptake by Glu-134 of the conserved E(D)RY motif at the cytoplasmic terminus of H3 (14), forming a salt bridge with Arg-135 that is part of an interhelical network between H3 and H6 in the cytoplasmic domain. Protonation of Glu-134 in Meta II from the solvent has been shown recently by FTIR spectroscopy (15). This second protonation switch leads to the anomalous pH-dependence of the Meta I/Meta II conformational equilibrium, favoring deprotonation of the PSB and the transition to active Meta II at acidic pH (16, 17).

By using rhodopsin purified in flexible detergents such as dodecyl maltoside, Hofmann and coworkers (14, 18) showed by kinetic UV–visible spectrophotometry and proton-uptake experiments that the transition from Meta I to Meta II proceeds in a sequential manner, with Schiff base deprotonation preceding the cytoplasmic proton uptake reaction, resulting in multiple Meta II states. Hubbell and collaborators (19) recently extended this scheme by using time-resolved EPR spectroscopy of spin-labeled detergent-solubilized rhodopsin, revealing that Meta $II_a$ converts to Meta $II_b$ by movement of H6, and to Meta $II_bH^+$ by the cytoplasmic proton uptake (Fig. 1*B*). Notably, the activating helix movements in the transition to Meta $II_b$ take place independently of pH and, hence, the proton uptake step under these conditions. This behavior differs considerably from the classical anomalous pH dependence of the Meta I/Meta II equilibrium in native membranes (16, 17), reflecting a substantial perturbation of the energetics of the metarhodopsin equilibrium induced by the detergent. Alternative models include a branched scheme where early intermediates with a protonated or deprotonated Schiff base evolve in a parallel manner on the time scale of Lumi decay (20).

Here, we develop a comprehensive thermodynamic model that allows the description of rhodopsin activation in both detergent and membrane environments within a single conceptual framework. We start from the extended scheme derived for rhodopsin in detergent (Fig. 1*B*) (18, 19) and treat the transition from Meta I to Meta $II_bH^+$ as a set of coupled equilibria with corresponding thermodynamic parameters. For native membranes, this reaction scheme reproduces the classical Henderson–Hasselbalch-like equilibrium between Meta I and Meta $II_bH^+$ at lower temperatures. At higher temperatures, more

Author contributions: M.F.B. and R.V. designed research; M.M., K.M.-M., and R.V. performed research; K.M.-M. contributed new reagents/analytic tools; M.M. and R.V. analyzed data; and M.F.B. and R.V. wrote the paper.

The authors declare no conflict of interest.

This article is a PNAS Direct Submission.

[1]To whom correspondence may be addressed. E-mail: mfbrown@u.arizona.edu.

[2]To whom correspondence may be addressed at: Biophysics Section, Institute of Molecular Medicine and Cell Research, Albert Ludwigs University, Hermann-Herder-Strasse 9, D-79104 Freiburg, Germany. E-mail: reiner.vogel@biophysik.uni-freiburg.de.

This article contains supporting information online at www.pnas.org/cgi/content/full/0804541105/DCSupplemental.

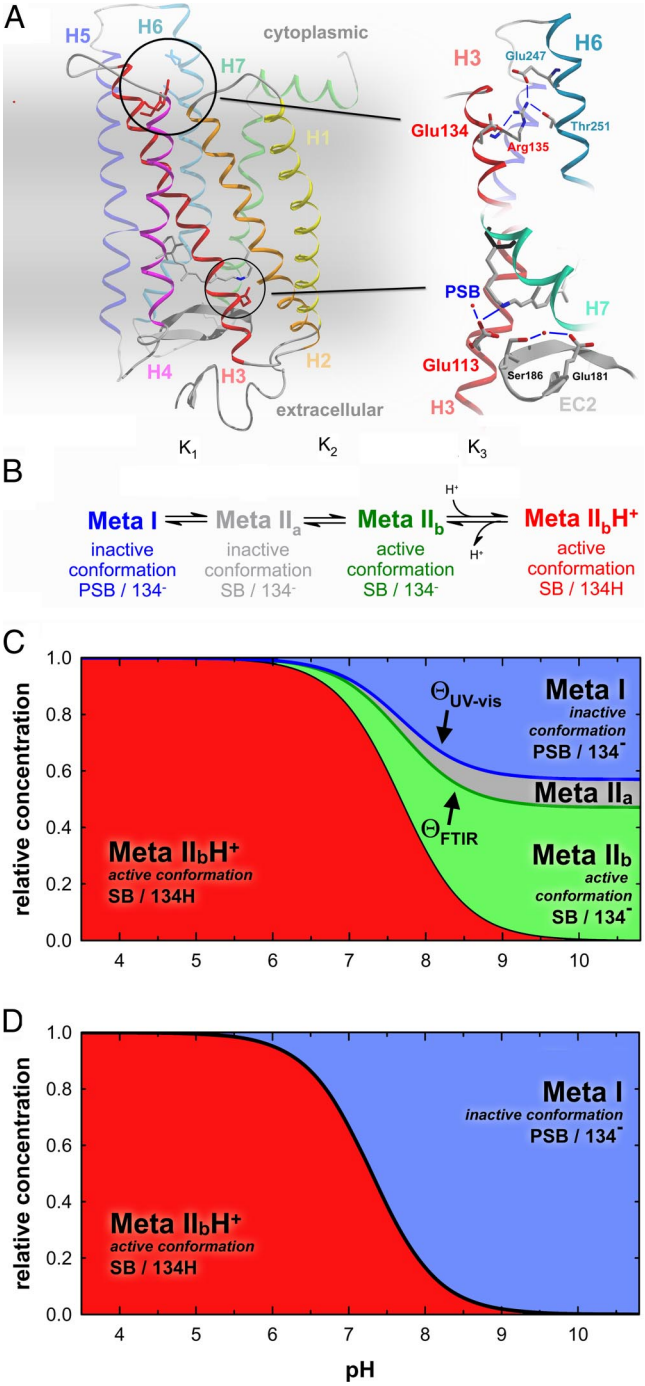


**Fig. 1.** Thermodynamic and structural model for rhodopsin activation in a membrane environment. (*A*) The structure of the dark state of rhodopsin [based on Protein Data Bank ID code 1GZM (25)] includes 2 protonation switches. The cytoplasmic network around Glu-134 in the ERY motif of H3 is involved in proton uptake from the solvent, and the interhelical salt bridge between the protonated retinal Schiff base (PSB) linked to H7 and Glu-113 on H3 in the transmembrane domain is disrupted by internal proton transfer during receptor activation. (*B*) Previous studies (14, 18, 19) have proposed a sequential reaction scheme of coupled equilibria of photoproduct states for rhodopsin activation in a detergent environment, involving PSB deprotonation in the transition to Meta $II_a$, activating helix movements in the transition to Meta $II_b$, and cytoplasmic proton uptake by Glu-134 in the transition to Meta $II_bH^+$. (The terms inactive and active are used to describe the receptor conformations before and after helix movements, respectively, and do not necessarily specify activity toward G protein.) (*C*) This reaction scheme predicts a complex titration behavior of photoproducts in a membrane environment, with Meta I, Meta $II_a$, and Meta $II_b$ forming an equilibrium at alkaline pH. This intrinsically pH-independent equilibrium is coupled to a pH-dependent equilibrium with Meta $II_bH^+$ at lower pH, reflecting proton uptake by Glu-134 from the solvent. (*D*) Because Meta $II_a$ and Meta $II_b$ are populated only at higher temperature, this 4-state scheme reduces to the classical 2-state Meta I/Meta $II_bH^+$ scheme at lower temperature.

complex titration curves are predicted with non-zero alkaline endpoints, reflecting in particular a significant population of the entropy-stabilized Meta $II_b$ state. The validity of this framework is tested and verified experimentally by using a combination of UV–visible and FTIR spectroscopy of rhodopsin in native and synthetic membranes, by which deprotonation of the PSB and activating conformational changes of the helix bundle can be accessed separately. These data are used to define the function of the second switch, protonation of Glu-134, which is shown to be a thermodynamic prerequisite to achieving full receptor activation in a membrane environment.

## Results

**Thermodynamic Model of Receptor Activation.** Starting from the extended model shown in Fig. 1*B* (18, 19), we first derive a titration scheme involving the different photoproduct species. At very alkaline pH, where the proton uptake by Glu-134 and, hence, formation of Meta $II_bH^+$ is absent, the extended reaction scheme is reduced to Meta I, Meta $II_a$, and Meta $II_b$, which form a set of 2 coupled, pH-independent equilibria. At lower pH, these intrinsically pH-independent equilibria are coupled to the pH-dependent equilibrium with Meta $II_bH^+$, resulting in the complex titration behavior shown in Fig. 1*C*.

Previous studies of the activation of rhodopsin analogues in membranes have suggested that disruption of the PSB salt bridge as the first protonation switch involves a relatively large unfavorable enthalpy change $\Delta H°$, which is only partially offset by a favorable positive entropy change $T\Delta S°$ (21, 22). The resulting free energy change $\Delta G° = \Delta H° - T\Delta S°$ for the first switch is compensated by the favorable $\Delta H°$ of the second switch, protonation of Glu-134, such that the transition to Meta II is strictly coupled to cytoplasmic proton uptake. At lower temperature, this coupling therefore reduces the extended scheme to the classical 2-state equilibrium between Meta I and Meta $II_bH^+$ (Fig. 1*D*). At higher temperature, because of the explicit temperature dependence of the entropic contribution to the free–energy change, triggering of the first switch should become favorable and, thus, independent of the second switch. With increasing temperature, we would therefore expect the classical 2-state equilibrium of Fig. 1*D* to evolve into the full 4-state equilibrium depicted in Fig. 1*C*.

**Schiff Base Deprotonation in the Meta I/Meta II Equilibria in Native Membranes.** By using UV–visible spectrophotometry, the protonation state of the Schiff base in the photoproducts can be determined as can the concentration of the Meta II states. The Meta I photoproduct with PSB absorbs at 485 nm, whereas the Meta II states with deprotonated Schiff base absorb at 380 nm (Fig. 2 *A* and *B*). The contribution of Meta II states with deprotonated Schiff base, $\Theta_{UV-vis}$, to the photoproduct equilibrium can be monitored in the photoproduct minus dark state difference spectra in Fig. 2*C* by decomposing them into a linear combination of difference spectra corresponding to the transitions to pure Meta I and Meta II states. At 10 °C, the resulting titration curve follows closely a regular Henderson–Hasselbalch function $\Theta_{UV-vis} = 10^{pKa-pH}/(1 + 10^{pKa-pH})$ with acidic and alkaline endpoints at 1 and 0, respectively, reflecting the classical 2-state equilibrium between Meta I and Meta $II_bH^+$ (Fig. 2*E*, green curve).

However, in the temperature range from 20 to 37 °C, the 380-nm absorption of Meta II persists even at very alkaline pH (Fig. 2*D*), and the titration curves follow the modified phenom-

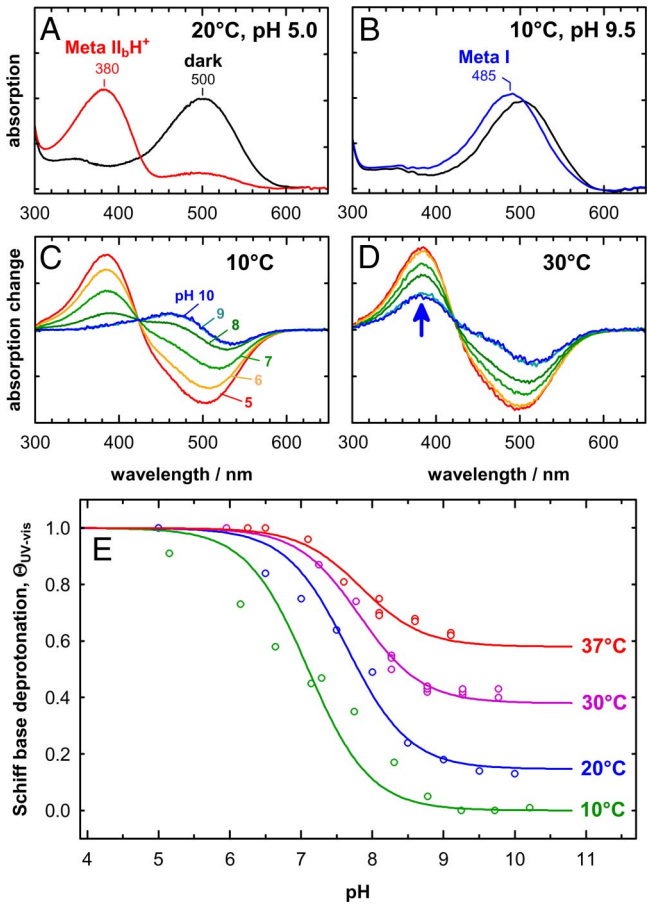


**Fig. 2.** UV–visible spectroscopic characterization of the PSB salt bridge in the Meta I/Meta II equilibrium in native disk membranes. (*A* and *B*) At 20 °C and pH 5.0, photolysis converts the dark state of rhodopsin (black) to the Meta $II_bH^+$ photoproduct state with deprotonated Schiff base (red), whereas, at 10 °C and pH 9.5, the Meta I photoproduct with protonated Schiff base (blue) is formed. (*C*) Difference spectra for the photoproduct minus dark state obtained at 10 °C reveal the pH dependence of the Meta I/Meta $II_bH^+$ equilibrium, which is completely on the side of Meta $II_bH^+$ at pH 5.0 and of Meta I at pH 9.0 and 10.0, as evident from the complete lack of absorption at 380 nm. (*D*) At 30 °C, the equilibrium is not fully shifted to Meta I at alkaline pH; instead a 380-nm Meta II photoproduct contribution is observed at very alkaline pH, which becomes pH-independent at pH 9.0 and above. (*E*) Schiff base deprotonation ($\Theta_{UV-vis}$) and, hence, the fraction of Meta II were determined from UV–visible difference spectra. At 10 °C the titration curve follows a regular Henderson–Hasselbalch function, whereas, at higher temperature, the alkaline endpoint $\Theta^{alk}_{UV-vis}$ does not reach zero because of increasing population of the Meta $II_a$ and Meta $II_b$ states.

enological function $\Theta_{UV-vis} = (\Theta^{alk}_{UV-vis} + 10^{pKa-pH})/(1 + 10^{pKa-pH})$, with non-zero values for $\Theta^{alk}_{UV-vis}$, the alkaline endpoint values of the titration curves (Fig. 2*E*). In the scheme depicted in Fig. 1*C*, $\Theta_{UV-vis}$ corresponds to the blue line and the alkaline endpoint value $\Theta^{alk}_{UV-vis}$ is determined by the combined contributions of Meta $II_a$ and Meta $II_b$ to the photoproduct equilibrium [see supporting information (SI) *Appendix*, text].

As our experiments involved a combination of elevated temperature and extremely alkaline pH values, photoproduct stability needed to be controlled carefully. We minimized the sampling time after photolysis in both UV–visible spectroscopy and FTIR experiments (see *Materials and Methods*) by using a 100-ms photolysis pulse followed by time-resolved spectral acquisition over 240-ms intervals. Consecutively recorded spectra verified the photoproduct stability in the initial spectra obtained immediately after photolysis and allowed spectral averaging (*SI Appendix*, Fig. S1).

**Changes in Interhelical Hydrogen-Bonded Networks in the Meta I/Meta II Equilibria in Native Membranes.** Whereas UV–visible spectrophotometry determines the protonation state of the retinal Schiff base, FTIR difference spectroscopy can be used to follow the conformation of the receptor in the photoproduct equilibria. FTIR difference spectra photoproduct minus dark state of rhodopsin in native disk membranes are decomposed into a linear combination of Meta I and Meta $II_bH^+$ reference (basis) spectra, as shown in Fig. 3*A*, corresponding to inactive and active receptor states, respectively. This decomposition yields $\Theta_{FTIR}$ as the fraction of the active conformation in the photoproduct equilibrium. Spectral decomposition was performed in the conformationally most sensitive spectral region between 1,800 and 1,600 $cm^{-1}$ (marked in green). This range comprises the amide I vibrations of the protein backbone and the C═O stretch of protonated carboxylic acids Glu-122 and Asp-83, which are involved in hydrogen-bonded networks between H3 and H5 and between H1, H2, and H7, respectively (11, 23–25), and are sensitive markers for the conformational changes during receptor activation (12, 26–28).

The titration curve follows a regular Henderson–Hasselbalch function at 10 °C but not at higher temperature, where the alkaline endpoint value, $\Theta^{alk}_{FTIR}$, is different from zero (Fig. 3*B*). Notably, at 30 and 37 °C, $\Theta^{alk}_{FTIR}$ is slightly lower than $\Theta^{alk}_{UV-vis}$. According to the reaction scheme in Fig. 1*C*, $\Theta^{alk}_{FTIR}$ corresponds to the contribution of Meta $II_b$ at alkaline pH. The small difference between $\Theta^{alk}_{UV-vis}$ and $\Theta^{alk}_{FTIR}$ therefore determines the contribution of Meta $II_a$ to the photoproduct equilibrium at the alkaline endpoint, amounting to only ≈11% at 37 °C and even less at lower temperatures. Alkaline endpoint and apparent $pK_a$ values are included in *SI Appendix*, Table S1.

**Rhodopsin Activation in Synthetic 1-Palmitoyl-2-Oleoyl-*sn*-Glycero-3-Phosphocholine (POPC) Membranes.** We also extended the experiments to rhodopsin reconstituted into POPC membranes (Fig. 3*C*), which differ from native disk membranes in the composition of both head groups and chains. These recombinant membranes reveal a generally similar titration scheme as native membranes, yet with drastic shifts in the associated equilibria, in agreement with previous studies (29, 30). The presence of an alkaline plateau region in POPC membranes as observed here deviates from results of a previous study that used a considerably longer acquisition time of ≈60 s after illumination (31), such that photoproduct instability might have distorted the data obtained at very alkaline pH. Interestingly, although the alkaline endpoint values in POPC recombinant membranes are only slightly lower, corresponding to shifts of the associated equilibrium constants by a factor of <2, the apparent $pK_a$ values of the titration curves are reduced by ≈1.5 units, corresponding to a downshift of the apparent protonation-dependent equilibrium constants by a factor of ≈30.

**Protonated and Unprotonated Meta $II_b$ Share a Similar Active State Receptor Conformation.** Neglecting the small contribution of Meta $II_a$, the alkaline endpoint FTIR difference spectra represent primarily the transition from the dark state to the Meta I/Meta $II_b$ photoproduct equilibrium. In Fig. 4, we compare these spectra with synthetic Meta I/Meta $II_bH^+$ minus dark state spectra calculated as a linear combination of the corresponding reference spectra obtained at 10 °C. The remarkable agreement between synthetic and experimental spectra indicates similar FTIR signatures of Meta $II_b$ and Meta $II_bH^+$. This agreement includes in particular the intense bands of conformationally sensitive carboxylic acids above 1,700 $cm^{-1}$ (and hence the H3/H5 and H1/H2/H7 interhelical networks as detailed above) and the amide I marker band of Meta II at 1,644 $cm^{-1}$. Note that the FTIR signature of protonation of Glu-134 should contribute to Meta $II_bH^+$ but not to Meta $II_b$. This pattern consists of a

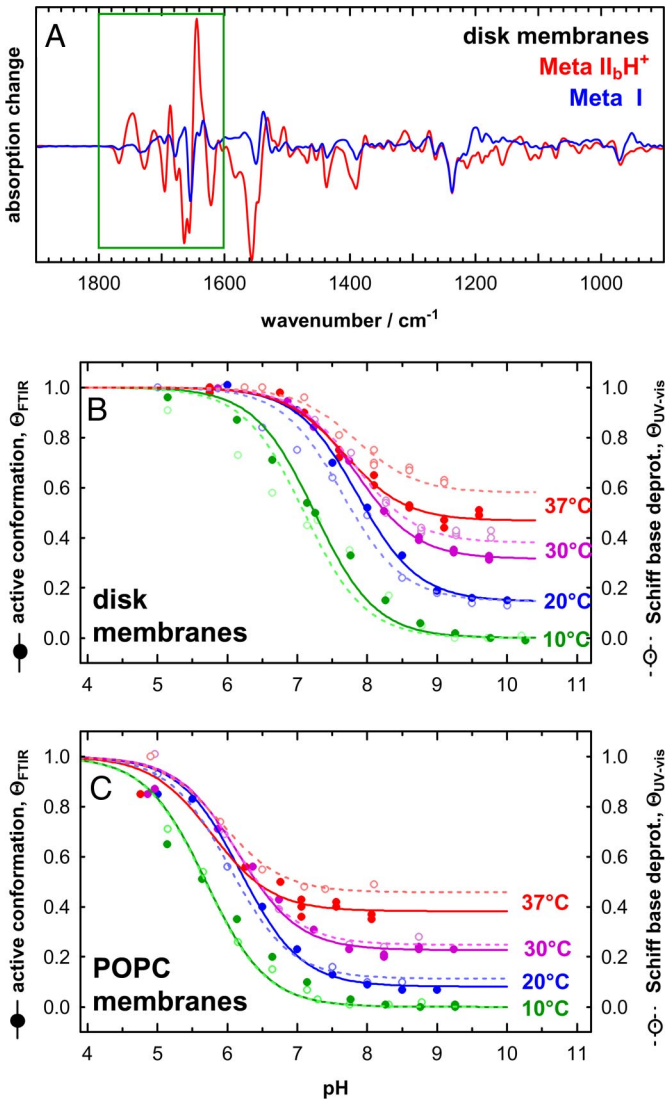


**Fig. 3.** FTIR spectroscopic characterization of activating conformational changes in the Meta I/Meta II equilibrium in native disk membranes. (*A*) Meta I and Meta $II_bH^+$ minus dark state FTIR difference spectra were obtained from rhodopsin in native disk membranes at 10 °C at pH 9.5 and 20 °C at pH 5.0, respectively, under identical conditions as in Fig. 2 *A* and *B*. By using the conformationally sensitive range marked in green, they served as basis spectra for inactive and active conformations, respectively, to determine the pH dependence of activating conformational changes. (*B*) The FTIR-based titration curves of receptor conformation, $\Theta_{FTIR}$ (filled circles and solid lines), reveal a similar deviation from classical Henderson–Hasselbalch behavior as the UV–visible data, with a temperature-dependent increase of the alkaline endpoint $\Theta^{alk}_{FTIR}$. The alkaline endpoints $\Theta^{alk}_{UV-vis}$ of the UV–visible-based titration curves (open symbols, broken lines, reproduced from Fig. 2*E*) at 30 and 37 °C are slightly higher than $\Theta^{alk}_{FTIR}$, revealing the additional contribution of inactive Meta $II_a$. (*C*) Rhodopsin reconstituted into synthetic POPC membranes shows the same general activation scheme but with shifted equilibria because of altered properties of the lipid bilayer. Both in native disk membranes and synthetic POPC membranes, proton uptake by Glu-134 and, hence, the transition to protonated Meta $II_bH^+$ is necessary for full receptor activation.

positive band at 1,713 $cm^{-1}$ and negative bands at 1,562 and 1,394 $cm^{-1}$ (15), which are small compared with the pronounced spectral changes of Asp-83, Glu-122, and Glu-113 (13, 26), and are therefore not clearly resolved in this approximation.

**Thermodynamic Parameters of the Meta I/Meta II Equilibria.** The equilibrium constants $K_1$, $K_2$, and $K_3$ of the single equilibria (Fig. 1*B*) can be expressed in terms of the experimental data $\Theta_{UV-vis}$ and $\Theta_{FTIR}$ as derived in *SI Appendix*, text. Free-energy changes were calculated at 37 °C from $\Delta G^\circ_i = -RT \ln K_i$, for the individual equilibria, with $R$ being the gas constant and $T$ the absolute temperature. This calculation indicates an increase of $G^\circ$ in disk membranes by ≈3.1 ± 1.9 kJ·$mol^{-1}$ in the transition from Meta I to Meta $II_a$ and a subsequent decrease by −3.7 ± 1.6 kJ·$mol^{-1}$ in the transition to Meta $II_b$ (4.6 ± 2.3 kJ·$mol^{-1}$ and −4.0 ± 2.5 kJ·$mol^{-1}$, respectively, in POPC membranes). The large errors reflect the uncertainty in determining a precise value of the low amount of Meta $II_a$ present. Values of $pK_{a3}$ of the Meta $II_b$ + $H^+ \leftrightarrows$ Meta $II_bH^+$ proton uptake reaction were determined to be 8.0 in native and 6.2 in recombinant POPC membranes (at 37 °C). Note that $pK_{a3}$ is different from the apparent $pK_a$ in the phenomenological Henderson–Hasselbalch description used above (see *SI Appendix*, text). This result yields a $\Delta G^\circ_3$of −48 ± 2 kJ·$mol^{-1}$ for disk membranes and −37 ± 2 kJ·$mol^{-1}$ for POPC membranes by using the solute standard state including the hydronium concentration. Furthermore, $\Delta H^\circ$ and $\Delta S^\circ$ values of the equilibria could not be obtained from the thermodynamic description of the full scheme because of the marginal population of Meta $II_a$. We therefore used a reduced reaction scheme in which the transition from Meta I to Meta $II_b$ was treated as a single step with an equilibrium constant $K_{12}$, neglecting the small contribution of Meta $II_a$. The $\Theta_{UV-vis}$ and $\Theta_{FTIR}$ data were then merged and $K_{12}$ was obtained by a fit to the observables. The free-energy change was calculated as $\Delta G^\circ_{12} = \Delta H^\circ_{12} - T\Delta S^\circ_{12} = -RT \ln K_{12}$, yielding $\Delta H^\circ_{12}$ = 88 ± 16 kJ·$mol^{-1}$ and $\Delta S^\circ_{12}$ = 285 ± 53 J·$mol^{-1}$·$K^{-1}$ (84 ± 22 kJ·$mol^{-1}$ and 269 ± 74 J·$mol^{-1}$·$K^{-1}$, respectively, in the case of POPC membranes) from a van 't Hoff analysis. The relatively large errors are because of the small

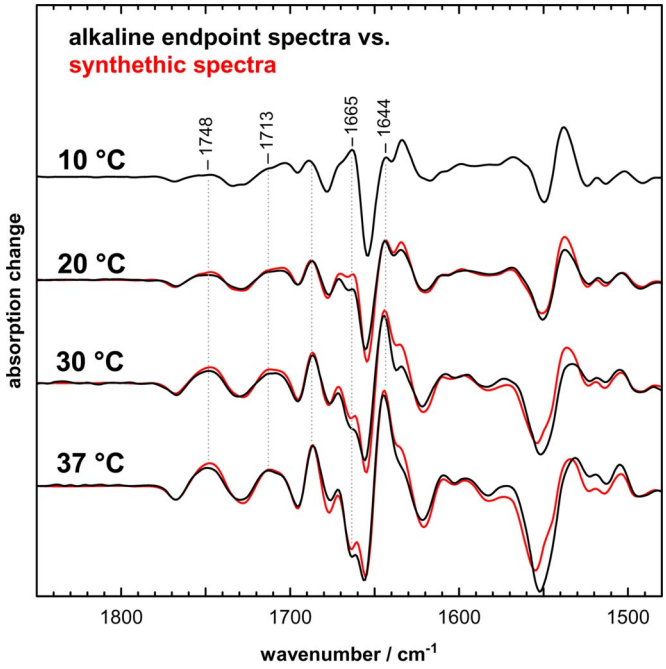


**Fig. 4.** Meta $II_b$ and Meta $II_bH^+$ share a similar active state FTIR signature. FTIR difference spectra for the photoproduct minus dark state obtained for disk membranes at the alkaline endpoint reveal the increasing contribution of the active conformation of unprotonated Meta $II_b$ to the Meta I/Meta $II_a$/Meta $II_b$ photoproduct equilibrium at higher temperature. Synthetic Meta I/Meta $II_bH^+$ minus dark state spectra (red) were calculated as a linear combination of the Meta I and Meta $II_bH^+$ basis spectra shown in Fig. 3*A* by using the endpoint values $\Theta^{alk}_{UV-vis}$ (neglecting the small contribution of Meta $II_a$). These synthetic spectra show a remarkable agreement with the experimental endpoint spectra, indicating similar FTIR signatures of Meta $II_b$ and Meta $II_bH^+$.

temperature range of the data between 20 and 37 °C. Additionally, $\Delta G^{\circ}_{3}$ consists primarily of a negative enthalpic term corresponding to a decrease of $pK_{a3}$ with increasing temperature. A more precise analysis is, however, precluded by large error margins imposed by the limited temperature range of the van't Hoff analysis.

## Discussion

**Activation Mechanism of Rhodopsin in Native Membranes.** In this study we have investigated the role of the 2 protonation switches for the activation of rhodopsin in its native membrane environment in the physiologically relevant temperature range. With UV–visible spectroscopy, we monitored the internal proton transfer leading to disruption of the PSB salt bridge, whereas FTIR spectroscopy allowed us to follow the conformational rearrangement of transmembrane helical networks during receptor activation. Moreover, the pH dependence of the spectral changes allowed us to map these changes to the cytoplasmic proton uptake step by Glu-134. We show that, at lower temperatures, exclusive triggering of the PSB-Glu-113 switch is disfavored and depends on the enthalpically downhill cytoplasmic proton uptake by Glu-134. This assistance by the Glu-134 protonation switch previously was shown to be facilitated by an allosteric coupling mechanism depending on the C9-methyl group and the $\beta$-ionone ring of all-*trans* retinal (22, 27, 28, 32). Coupling of the 2 protonation switches establishes the classical 2-state equilibrium between Meta I and protonated Meta $II_bH^+$ (16, 17) at 10 °C and below. As a key result, we show that at higher temperatures the 2 switches become partially uncoupled, leading to population of the unprotonated Meta $II_b$ state (and a marginal population of Meta $II_a$), in which the PSB–Glu-113 salt bridge is broken, but cytoplasmic proton uptake by Glu-134 is absent (see Fig. 1).

**Role of Glu-134 Protonation for Conformational Changes in Rhodopsin Activation.** Glu-134 is part of the conserved E(D)RY and, in the dark state, forms an intrahelical salt bridge with neighboring Arg-135 at the cytoplasmic terminus of H3 (Fig. 1*A*) (23–25). A similar intrahelical salt bridge is assumed to control activation of other GPCRs (33) and also is present in the recently solved adrenergic receptor structures (34–36). Neutralization of position 134 in the E134Q rhodopsin mutant abolishes proton uptake during Meta II formation (14) and leads to pH-independent Meta II formation even in a membrane environment (15, 22). In our studies on rhodopsin in membranes, both unprotonated Meta $II_b$ and protonated Meta $II_bH^+$ are shown to share a very similar active receptor conformation, despite their differing protonation states regarding the Glu-134 switch. This finding agrees with previous studies on detergent-solubilized rhodopsin, showing that activating movement of H6 require disruption of the PSB salt bridge (37) but are not per se dependent on proton uptake by Glu-134 (19).

What, then, is the role of protonation of Glu-134? Protonation of Glu-134 is enthalpically downhill, as shown here and in previous studies (18) and renders more favorable an electrostatically unfavorable environment in the cytoplasmic H3/H6 microdomain. This view is supported by the $pK_{a3}$ of 8.0 for the proton uptake reaction, which is substantially higher than the $pK_a < 5$ of a carboxylate in solution. Such a hydrophobic environment could be created by a movement of Arg-135 away from Glu-134 in Meta II, in keeping with the recently solved structure of the active conformation of opsin (11). Notably, in the native membrane environment, the proton uptake function of Glu-134 also is relevant at 37 °C, where the pH-independent conformational equilibrium between Meta I and Meta $II_b$ is only halfway on the active side. From an energetic point of view, protonation of Glu-134 is therefore a prerequisite for complete receptor activation under physiological conditions.

**Glu-134 Protonation and Signal Transduction.** Protonation of Glu-134 probably serves a dual role by additionally improving the binding of the activated receptor to the G protein. The E134Q mutation extends G protein activation of detergent-purified pigment into the alkaline range, although the detergent environment favors pH-independent Meta II formation already in the wild-type receptor (38). This finding suggests that a protonated Glu-134 sidechain facilitates productive interaction with the G protein transducin. Fluorescence spectroscopy has further revealed the H3/H6 microdomain to contribute to the binding site of the C-terminal part of the G protein $\alpha$-subunit (39). Because this C-terminal part of transducin contains three potentially charged carboxylates, protonation of Glu-134 on the receptor side would reduce electrostatic repulsion or allow a repositioning of neighboring Arg-135 to provide for efficient binding.

## Conclusions

We have analyzed the structural and thermodynamic roles of the 2 protonation switches that control activation of rhodopsin in its native membrane environment. We show that the transitions associated with disruption of the PSB salt bridge and proton uptake by the cytoplasmic ionic lock around Glu-134 become partially uncoupled under physiological conditions. This partial uncoupling allows formation of an entropy-stabilized Meta II state, in which the conformational changes associated with receptor activation have taken place despite the lack of protonation of Glu-134. Disruption of the salt bridge between the PSB and its complex counterion is therefore a structural prerequisite for the activating helix movements, whereas protonation of Glu-134 is a thermodynamic requirement for shifting the conformational equilibrium completely to the active Meta II conformation. Although the structural role of PSB salt-bridge disruption is similarly observed for rhodopsin in detergent (37), the thermodynamic function of the second switch is not required in a detergent environment (19) because of a lowered enthalpy change in the transition to Meta II. Therefore, in native and synthetic membranes, a sequential destabilization of both salt bridges is required for full receptor activation. The similar structure of the intrahelical salt bridge in the DRY motif in the adrenergic receptor structures (34–36) suggests a similar thermodynamic role of this second switch in the activation of other members of the rhodopsin-like receptor family.

## Materials and Methods

**Sample Preparation.** Rhodopsin in native hypotonically washed disk membranes was prepared from cattle retinae (Lawson) according to standard procedures (40). For experiments on recombinant membranes, rhodopsin was purified in dodecyltrimethylammonium bromide detergent and reconstituted into synthetic POPC lipid membranes according to published procedures (41). Experiments were performed with sandwich samples with 0.5 nmol of pigment (prepared as described in detail in ref. 21) by using 200 mM morpholinoethanesulfonic acid and bis-Tris propane buffer in overlapping pH ranges.

**FTIR Spectroscopy.** FTIR difference spectroscopy was performed with a Bruker Vertex 70 spectrometer with a mercury–cadmium–telluride detector. IR spectra were recorded by using time-resolved rapid-scan FTIR spectroscopy with a spectral resolution of 4 $cm^{-1}$. An acquisition time of 6 s was used for the preillumination spectrum and a time of 240 ms for the single postillumination spectra. Alternatively, at 10 and 20 °C, conventional FTIR difference spectroscopy was used with acquisition times of 12 s for preillumination spectra and between 1.5 and 12 s for postillumination spectra, depending on temperature and stability of the photoproduct states. In all experiments, thermal stability of the photoproduct states was confirmed in series of postillumination spectra (see *SI Appendix*, Fig. S1). Samples were photolyzed with an array of 6 ultrabright green ($\lambda_{max}$, 520 nm) 5-mm LEDs (Nichia) with nominal 16 candela at 20-mA current and 15° emission half angle. Illumination time was 100 ms at 100 mA in rapid scan experiments, by which ≈70% of rhodopsin was photolyzed. By using its fingerprint bands as spectral markers, the contribution of isorhodopsin to the photoproduct equilibria was found to be small under

these conditions (≈10% of that of Meta I). The resulting small overestimation of the Meta I contribution was accounted for in the calculation of $\Delta G°$ values. In conventional FTIR experiments, illumination was 2 s at 20 mA, which led to complete photolysis. Spectral normalization was achieved by using the intense 1,237-$cm^{-1}$ fingerprint mode of the dark state; contributions of overlapping buffer bands in this range were corrected as detailed previously (15). FTIR-based titration curves were derived as described in ref. 27. Reference spectra for Meta $II_bH^+$ and Meta I were obtained at 20 °C at pH 5.0 and at 10 °C at pH 9.5, respectively. Spectra obtained by conventional FTIR spectroscopy and by rapid-scan FTIR spectroscopy were evaluated separately by using separate sets of reference spectra acquired with the respective illumination protocol. POPC samples were evaluated with a separate set of basis spectra. In this case, the active-state basis spectrum was obtained from rhodopsin reconstituted in 1,2-dioleoyl-*sn*-glycero-3-phosphocholine, accounting for the difficulties in obtaining a pure Meta II spectrum in POPC.

**UV–Visible Spectroscopy.** UV–visible spectroscopy was performed with a Hewlett Packard 8453 diode array spectrometer using a neutral density filter with 10% transmission to minimize sample bleaching by the measuring beam. Spectral acquisition time was 1 s at 10 and 20 °C and 200 ms at 30 and 37 °C. Sample and illumination conditions were identical to the FTIR experiments. UV–visible-based titration curves and FTIR-based curves were calculated in similar ways by decomposing the measured UV–visible difference spectra into a linear combination of reference spectra for the transition to pure Meta I and Meta II states, respectively, obtained under conditions similar to those in the FTIR experiments.

**ACKNOWLEDGMENTS.** We thank the reviewers for helpful comments, and R.V. thanks Fritz Siebert for support. This work was supported by National Institutes of Health Grants EY12049 and EY18891 (to M.F.B.) and Deutsche Forschungsgemeinschaft Grant Vo 811/3-4 and 4-1 (to R.V.).

1. Samama P, Cotecchia S, Costa T, Lefkowitz RJ (1993) A mutation-induced activated state of the beta 2-adrenergic receptor. Extending the ternary complex model. *J Biol Chem* 268:4625–4636.
2. Menon ST, Han M, Sakmar TP (2001) Rhodopsin: Structural basis of molecular physiology. *Physiol Rev* 81:1659–1688.
3. Lewis JW, Kliger DS (2000) Absorption spectroscopy in studies of visual pigments: Spectral and kinetic characterization of intermediates. *Methods Enzymol* 315:164–178.
4. Shichida Y, Imai H (1998) Visual pigment: G-protein-coupled receptor for light signals. *Cell Mol Life Sci* 54:1299–1315.
5. Struts AV, *et al.* (2007) Structural analysis and dynamics of retinal chromophore in dark and meta I states of rhodopsin from $^2H$ NMR of aligned membranes. *J Mol Biol* 372:50–66.
6. Salgado GF, *et al.* (2006) Solid-state $^2H$ NMR structure of retinal in metarhodopsin I. *J Am Chem Soc* 128:11067–11071.
7. Schertler GFX (2005) Structure of rhodopsin and the metarhodopsin I photointermediate. *Curr Opin Struct Biol* 15:408–415.
8. Sheikh SP, Zvyaga TA, Lichtarge O, Sakmar TP, Bourne HR (1996) Rhodopsin activation blocked by metal-ion-binding sites linking transmembrane helices C and F. *Nature* 383:347–350.
9. Altenbach C, Kusnetzow AK, Ernst OP, Hofmann KP, Hubbell WL (2008) High-resolution distance mapping in rhodopsin reveals the pattern of helix movement due to activation. *Proc Natl Acad Sci USA* 105:7439–7444.
10. Farrens DL, Altenbach C, Yang K, Hubbell WL, Khorana HG (1996) Requirement of rigid-body motion of transmembrane helices for light activation of rhodopsin. *Science* 274:768–770.
11. Park JH, Scheerer P, Hofmann KP, Choe HW, Ernst OP (2008) Crystal structure of the ligand-free G-protein-coupled receptor opsin. *Nature* 454:183–187.
12. Lüdeke S, *et al.* (2005) The role of Glu 181 in the photoactivation of rhodopsin. *J Mol Biol* 353:345–356.
13. Jäger F, Fahmy K, Sakmar TP, Siebert F (1994) Identification of glutamic acid 113 as the Schiff base proton acceptor in the Metarhodopsin II photointermediate of rhodopsin. *Biochemistry* 33:10878–10882.
14. Arnis S, Fahmy K, Hofmann KP, Sakmar TP (1994) A conserved carboxylic acid group mediates light-dependent proton uptake and signaling by rhodopsin. *J Biol Chem* 269:23879–23881.
15. Vogel R, *et al.* (2008) Functional role of the ''ionic lock''—an interhelical hydrogen-bond network in family A heptahelical receptors. *J Mol Biol* 380:648–655.
16. Matthews RG, Hubbard R, Brown PK, Wald G (1963) Tautomeric forms of Metarhodopsin. *J Gen Physiol* 47:215–240.
17. Parkes JH, Liebman PA (1984) Temperature and pH dependence of the Metarhodopsin I - Metarhodopsin II kinetics and equilibria in bovine rod disk membrane suspensions. *Biochemistry* 23:5054–5061.
18. Arnis S, Hofmann KP (1993) Two different forms of Metarhodopsin II: Schiff base deprotonation precedes proton uptake and signaling state. *Proc Natl Acad Sci USA* 90:7849–7853.
19. Knierim B, Hofmann KP, Ernst OP, Hubbell WL (2007) Sequence of late molecular events in the activation of rhodopsin. *Proc Natl Acad Sci USA* 104:20290–20295.
20. Thorgeirsson TE, Lewis JW, Wallace-Williams SE, Kliger DS (1993) Effects of temperature on rhodopsin photointermediates from lumirhodopsin to metarhodopsin II. *Biochemistry* 32:13861–13872.
21. Vogel R, *et al.* (2006) Modulating rhodopsin receptor activation by altering the $pK_a$ of the retinal Schiff base. *J Am Chem Soc* 128:10503–10512.
22. Vogel R, Sakmar TP, Sheves M, Siebert F (2006) Coupling of protonation switches during rhodopsin activation. *Photochem Photobiol* 83:286–292.
23. Palczewski K, *et al.* (2000) Crystal structure of rhodopsin: A G protein-coupled receptor. *Science* 289:739–745.
24. Okada T, *et al.* (2004) The retinal conformation and its environment in rhodopsin in light of a new 2.2 Å crystal structure. *J Mol Biol* 342:571–583.
25. Li J, Edwards PC, Burghammer M, Villa C, Schertler GFX (2004) Structure of bovine rhodopsin in a trigonal crystal form. *J Mol Biol* 343:1409–1438.
26. Fahmy K, *et al.* (1993) Protonation states of membrane-embedded carboxylic acid groups in rhodopsin and Metarhodopsin II: A Fourier-transform infrared spectroscopy study of site-directed mutants. *Proc Natl Acad Sci USA* 90:10206–10210.
27. Vogel R, Siebert F, Lüdeke S, Hirshfeld A, Sheves M (2005) Agonists and partial agonists of rhodopsin: Retinals with ring modifications. *Biochemistry* 44:11684–11699, and erratum (2005) 44:12914.
28. Vogel R, *et al.* (2006) Agonists and partial agonists of rhodopsin: Retinal polyene methylation affects receptor activation. *Biochemistry* 45:1640–1652.
29. Wang Y, Botelho AV, Martinez GV, Brown MF (2002) Electrostatic properties of membrane lipids coupled to metarhodopsin II formation in visual transduction. *J Am Chem Soc* 124:7690–7701.
30. Gibson NJ, Brown MF (1993) Lipid headgroup and acyl chain composition modulate the MI-MII equilibrium of rhodopsin in recombinant membranes. *Biochemistry* 32:2438–2454.
31. Botelho AV, Huber T, Sakmar TP, Brown MF (2006) Curvature and hydrophobic forces drive oligomerization and modulate activity of rhodopsin in membranes. *Biophys J* 91:4464–4477.
32. Meyer CK, *et al.* (2000) Signaling states of rhodopsin: Retinal provides a scaffold for activating proton transfer switches. *J Biol Chem* 275:19713–19718.
33. Kobilka BK (2007) G protein coupled receptor structure and activation. *Biochim Biophys Acta* 1768:794–807.
34. Rasmussen SG, *et al.* (2007) Crystal structure of the human beta-2 adrenergic G-protein-coupled receptor. *Nature* 450:383–387.
35. Warne T, *et al.* (2008) Structure of a $\beta_1$-adrenergic G-protein-coupled receptor. *Nature* 454:486–491.
36. Cherezov V, *et al.* (2007) High-resolution crystal structure of an engineered human beta2-adrenergic G protein-coupled receptor. *Science* 318:1258–1265.
37. Kim JM, *et al.* (2004) Structural origins of constitutive activation in rhodopsin: Role of the K296/E113 salt bridge. *Proc Natl Acad Sci USA* 101:12508–12513.
38. Fahmy K, Sakmar TP (1993) Regulation of the rhodopsin-transducin interaction by a highly conserved carboxylic acid group. *Biochemistry* 32:7229–7236.
39. Janz JM, Farrens DL (2004) Rhodopsin activation exposes a key hydrophobic binding site for the transducin $\alpha$-subunit C terminus. *J Biol Chem* 279:29767–29773.
40. Papermaster DS (1982) Preparation of retinal rod outer segments. *Methods Enzymol* 81:48–52.
41. Botelho AV, Gibson NJ, Thurmond RL, Wang Y, Brown MF (2002) Conformational energetics of rhodopsin modulated by nonlamellar-forming lipids. *Biochemistry* 41:6354–6368.